Elastic Modulus of Polyethylene in the Crystal Chain Direction As Measured by X-ray Diffraction

Masaru Matsuo* and Chie Sawatari

Department of Clothing Science, Faculty of Home Economics, Nara Women's University, Nara 630, Japan. *Received January 22, 1986; Revised Manuscript Received April 18, 1986*

ABSTRACT: The crystal lattice modulus of polyethylene was measured by X-ray diffraction using ultradrawn films that were produced by gelation/crystallization from dilute solution. The measurement was carried out at 20 °C for specimens with various elongation ratios beyond 50. The measurable crystal lattice modulus was in the range from 213 to 229 GPa and these values were independent of elongation ratios. This independence supports the assumption that the stress within a specimen is homogeneous. Furthermore, an effort was made to produce specimens whose Young's modulus is almost equal to the theoretical value. Through trial and error, it turned out that Young's modulus approached 216 GPa, nearly the theoretical limit of hardness, in the case that the dry gel films could be consistently elongated to the remarkably high draw ratio of 400.

Introduction

Polymer molecules are intrinsically anisotropic in physical properties (e.g., mechanical and optical). This intrinsic anisotropy causes the bulk properties of polymer aggregates to be anisotropic when the polymer molecules are oriented. In recent years, research on the preparation of fibers and films with high modulus and high strength has become a topic of increasing interest.[1-10] This research is based on the assumption that the theoretical Young's modulus and tensile strength of polymeric materials could be realized if the chains were fully aligned and extended and if the specimen is almost completely crystalline. In an attempt to produce such an ideal sample, chain alignment induced by deformation or flow has been extensively investigated. The ultimate value of Young's modulus is well-known to be equivalent to the crystal lattice modulus in the direction of the polymer chain axes. The study of the crystal lattice modulus has been concentrated on polyethylene and values have been reported as measured by X-ray diffraction (235 GPa),[11,12] Raman spectroscopy (290 GPa),[13] and inelastic neutron scattering (329 GPa).[14] The Raman and neutron values are significantly higher than that obtained by X-ray diffraction. This difference may be due to the essential problem of determining the crystal lattice modulus by Raman spectroscopy and inelastic neutron scattering. Namely, in addition to the difficulty in estimating lamellar length by small-angle X-ray scattering, both methods contain an unavoidable assumption concerning the frequency of absorption bands in a polymeric system. On the other hand, theoretical treatments of the crystal lattice modulus were reported by Odajima et al.[15] and Tashiro et al.[16] The calculated values, however, are different because of difficulties in estimating the effects of intermolecular interaction, which cannot be ignored.

X-ray diffraction measurements were carried out by Sakurada et al.[11,12] using several kinds of oriented polyethylene samples having different crystallinities and molecular weights. They concluded that the value of the crystal lattice modulus is independent of the above factors. However, an essential question arises as to whether the homogeneous stress is valid in such a case. That is, whether the stress within a specimen is everywhere the same as the external applied stress. If this hypothesis may be used, X-ray diffraction has the advantage of determining the crystal lattice modulus directly.

This paper is concerned with the estimation of the crystal lattice modulus in the direction of the molecular chain axis by X-ray diffraction measurements. Ultradrawn films with different elongation ratios such as 50, 100, 200, and 300 were used as specimens in order to check the homogeneous stress hypothesis. Furthermore we find that Young's modulus at 20 °C reaches the theoretical crystal lattice modulus when polyethylene films are elongated to a draw ratio of about 400.

Experimental Section

Sample Preparation and Characterization. The sample used in this experiment was linear polyethylene (Hercules 1900/90189) with an intrinsic viscosity of 30 dL/g, corresponding to a molecular weight of 6×10^6. The solvent was decalin. Gel films were prepared by crystallization from solution. A decalin solution containing 0.4 g/dL and 0.1 % (w/w) of the antioxidant di-*t*-butyl-*p*-cresol was prepared by heating the well-blended polymer/solvent mixture at 135 °C for 40 min under nitrogen.[9,10] The hot homogenized solution was quenched by pouring it into an aluminum tray that was surrounded by ice water, thus generating a gel. The decalin was allowed to evaporate from the gel under ambient conditions. The resulting 300-μm dry gel film was immersed in ethanol and subsequently air-dried to remove residual traces of the decalin–ethanol mixture.

The dry gel films were cut into strips 22 mm long and 10 mm wide. The strips were clamped in a manual stretching device in such a way that the length to be drawn was 4 mm. The specimens were placed in an oven at 135 °C and elongated manually to the desired draw ratio λ (less than 100). Immediately after stretching, in one case, the stretcher with the sample was quenched to room temperature for 30 min, and, in the other case, the stretcher with the sample was annealed at 110 °C for 60 min and cooled slowly to room temperature. This experimental procedure produced specimens with various crystallinities, allowing the study of the relationship between crystallinity and crystal lattice modulus. Draw ratios were determined in the usual way by measuring the displacement of ink marks placed 1 mm apart on the specimen prior to drawing. Due to the limited size of the oven, elongation beyond $\lambda = 100$ was done in two steps. The original 4 mm specimen was drawn to $\lambda = 50$ in the first step and the drawn film was cut into strips of 50-mm length. These specimens, each clamped over a length of 10 mm at the end (the length to be stretched being 30 mm) were drawn to the desired ratios beyond $\lambda = 100$. After stretching, some specimens were annealed and some specimens were quenched as discussed before.

The density of the film was measured by a pycnometer with chlorobenzene–toluene as a medium. Great care was taken to remove the antioxidant. Then, the drawn specimen was cut into fragments, immersed in ethanol for 30 days prior to measuring the density, and subsequently vacuum-dried for 1 day. The removal of the antioxidant was confirmed by infrared absorption.

Experimental Procedure. Figure 1 is a sketch showing the optical system of the wide-angle X-ray diffraction (WAXD) with a scintillation counter and 12-kW rotating anode X-ray generator (Rigaku RDA-rA operated at 200 mA and 40 kV). The intensity distribution measurement was carried out with point focusing under such a system that an incident beam was collimated by a collimator 2 mm in diameter and the diffraction beam was detected by a slit 0.9 mm × 0.9 mm. The incident beam was monochromatized by a curved graphite monochrometer. The

0024-9297/86/2219-2036$01.50/0

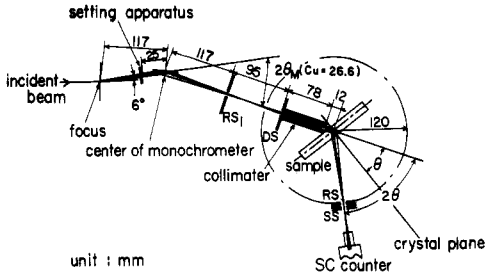

Figure 1. Wide-angle X-ray diffraction optical system used to detect the crystal lattice strain of the crystal (002) plane.

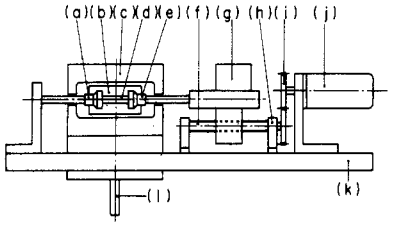

Figure 2. Stretching apparatus driven by a motor to ensure a constant tension: (a) fixed clamp, (b) Beryllium plate, (c) constant-temperature box, (d) sample, (e) movable clamp, (f) axis to stretch a test specimen, (g) mechanical detector, (h) ball bearing, (i) gear, (j) motor, (k) plate to fix mechanical parts, (l) rotational axis.

intensity distribution was measured with a step-scanning device at a step interval of 0.1°, each at a fixed time of 100 s, in the range from 71° to 79° (twice the Bragg angles).

Figure 2 shows the constant-tension stretching apparatus. The specimen was mounted horizontally in the stretching clamps and the crystal (002) plane was detected by the diffractometer shown in Figure 1. A load cell was fixed at the right end of the clamp. The load cell consists of a steel ring whose deformation during elongation is negligibly small compared to the specimen. The deformation of the ring due to the tensile strength of the specimen is electronically transformed as analogue voltage.

Figure 3 is a schematic diagram of the X-ray diffraction intensity distribution. Curves a and b show the intensity distribution from the crystal (002) plane plane in the undeformed and deformed states, respectively. The deviation of peak position was estimated as that of the center of gravity of the intensity distribution function as follows:

$$2\Delta\theta = 2\theta_{max} - 2\theta_{max}' \tag{1}$$

where

$$2\theta_{max} = \int_{2\theta_1}^{2\theta_2} 2\theta_B I(\theta_B) d\theta_B / \int_{2\theta_1'}^{2\theta_2'} I(\theta_B)\, d\theta_B \tag{2}$$

and

$$2\theta_{max}' = \int_{2\theta_1'}^{2\theta_2'} 2\theta_B I'(\theta_B)\, d\theta_B / \int_{2\theta_1'}^{2\theta_2'} I'(\theta_B)\, d\theta_B \tag{3}$$

where $I(\theta_B)$ and $I'(\theta_B)$ are the intensity distribution functions in the undeformed and deformed states, respectively, and $2\theta_{max}$ and $2\theta_{max}'$ are the corresponding average maxima concerning the diffraction peak positions. In actual calculation, $2\theta_1$ ($2\theta_1'$) and $2\theta_2$ ($2\theta_2'$) are chosen to be 71° and 79°. The crystal lattice strain ϵ_c is related to $\Delta\theta$ in eq 1, as follows:

$$\epsilon_c = -\cot \theta_{max} \Delta\theta \tag{4}$$

Thus, the crystal lattice modulus E_c is

$$E_c = \sigma/\epsilon_c \tag{5}$$

where σ is the applied stress due to the constant load.

Orientations of three crystallographic axes may be estimated by X-ray diffraction intensity distribution $I(2\theta_B, \theta_j, \phi_j)$ of the reciprocal lattice vector of the jth crystal plane. The angles θ_j and ϕ_j denote the polar and azimuthal angles with respect to the stretching direction. Since the crystallites have random orientation around the stretching direction, the intensity distribution function

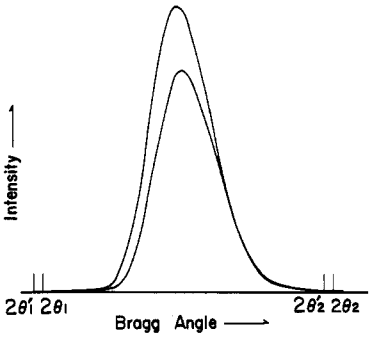

Figure 3. Schematic diagram of X-ray diffraction intensity distribution of the crystal (002) plane for (a) undeformed and (b) deformed specimens.

of the jth reciprocal lattice vector is independent of ϕ_j. Therefore we have

$$2\pi q_j(\cos\theta_j) = \frac{\int_{2\theta_1}^{2\theta_2} I(2\theta_B,\theta_j,\phi_j)\, d\theta_B}{\int_0^{\pi}\left[\int_{2\theta_1}^{2\theta_2} I(2\theta_B,\theta_j,\phi_j)\, d\theta_B\right] \sin\theta_j\, d\theta_j} \tag{6}$$

The function of $2\pi q_j(\cos\theta_j)$ is determined from $I(2\theta_B,\theta_j)$ by the integral of X-ray diffraction intensity distribution as a function of $2\theta_B$ for the equatorial direction as a fixed value of θ_j. The change in $2\pi q_j(\cos\theta_j)$ with θ_j may be determined by the rotation of the specimen around its thickness direction. Incidentally, the intensity distribution $I(2\theta_B,\theta_j)$ in eq 6 is obtained after applying a correction to the observed X-ray diffraction intensity (for air-scattering, polarization, and absorption) and substracting the contribution of the amorphous halo from the corrected total intensity curve. In the actual measurement, the contribution of air-scattering and amorphous halo were very small.

The second-order orientation factor F_{20}^j of the reciprocal lattice vector of the jth crystal plane is given by[17]

$$F_{20}^j = \frac{\int_0^{\pi} (1/2)(3\cos^2\theta_j - 1) q_j(\cos\theta_j) \sin\theta_j\, d\theta_j}{\int_0^{\pi} q_j(\cos\theta_j) \sin\theta_j\, d\theta_j} \tag{7}$$

The relationship between E_c and F_{20}^j shall be discussed later in detail.

In order to check the relationship between E_c and the crystal size $\bar{D}$ the half-width $\bar{\beta}$ was measured from the profile of the wide-range X-ray diffraction intensity distribution of the crystal (002) plane as a function of θ_B, and the crystal size was estimated by Scherrer's equation, which will be discussed elsewhere in detalil.[10]

The mechanical property of the bulk specimen was represented by the real part E' of the complex dynamic tensile modulus instead of Young's modulus, since E' is equivalent to an instantaneous (glassy) modulus which is slightly higher than Young's modulus at infinite frequency. The measurement was carried out over the range 0.1–100 Hz at 20 °C using a Iwamoto Machine Co. Ltd. (VES-F) viscoelastic spectrometer. The gage length of the specimen was 40 mm and the width was about 1.5 mm. In the actual measurement, the film was subjected to a static tensile strain corresponding to an initial stress of about 0.1 GPa in order to superpose dynamic strain of 0.025%.

Results and Discussion

Figures 4–7 show the relationship between the stress and the crystal lattice strain. The plots show a linear relationship in the range of small lattice strain except in the case of specimens B-1 and D-1. At large lattice strains, however, the plots tend to level off as shown in specimens A-2, C-2, C-4, and C-5. Such a relationship is characteristic of the mechanical behavior generally observed in bulk specimens. It may be noted that the crystal lattice modulus, determined at small lattice strains, ranges from 213 to 229 GPa for most of the specimens (except specimens

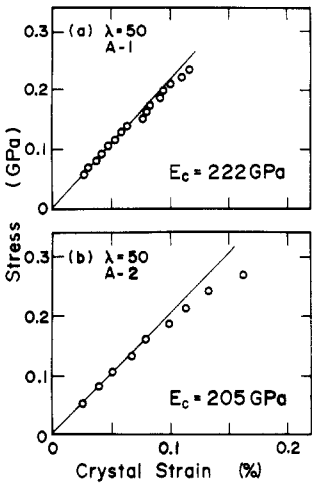

Figure 4. Stress–strain relationship for the crystal (002) plane for the specimen with the elongation ratio of $\lambda = 50$.

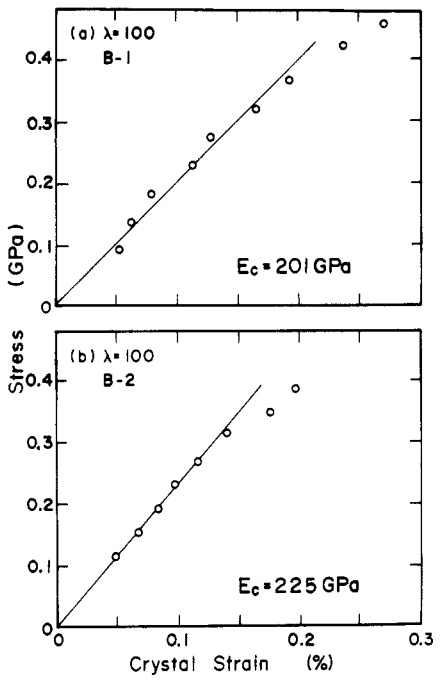

Figure 5. Stress–strain relationship for the crystal (002) plane for the specimen with the elongation ratio of $\lambda = 100$.

A-2, B-1, and D-1) and that these values are independent of elongation ratio λ. This indicates that the homogeneous stress hypothesis may be valid since the specimens with $\lambda \geq 50$ have a sufficiently high degree of crystal c axis alignment, as discussed below. All values listed in Figures 4–7 are slightly lower than reported by Sakurada et al. (235 GPa).[11,12] This discrepancy is probably due to the following two causes. The frist is the uncertainty in the linearization of the stress–lattice strain plots because the results of Sakurada et al. cannot be readily approximated by a straight line. The second is the variation of crystallinity and orientation of the crystal c axes in different samples. According to Sakurada's experiment,[11,12] necking around the center of the test specimen, where the incident X-ray beam was directed, became considerable at high elongation. In contrast, our results in Figures 4–7 are reasonable, because the crystallinity is higher than 90% and the orientation of the crystal c axes is almost perfect, as will be discussed later. Actually, the specimen elongation was found to be negligibly small during the measurement of crystal lattice strain. In such a condition, it may be postulated that the stress within the test specimen is equal

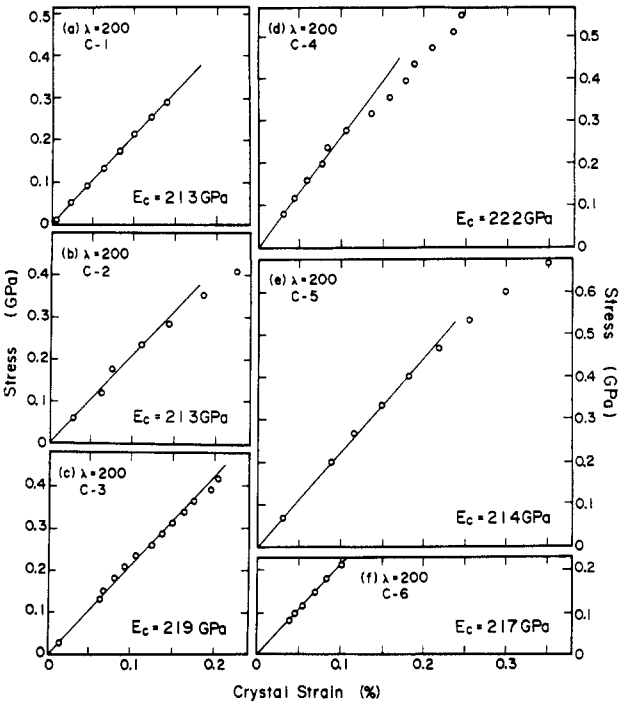

Figure 6. Stress–strain relationship for the crystal (002) plane for the specimen with the elongation ratio of $\lambda = 200$.

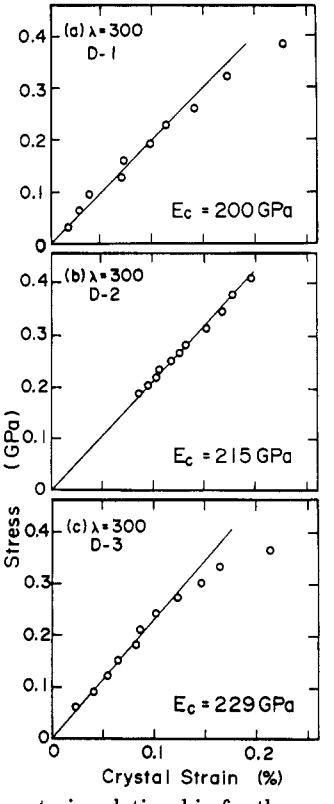

Figure 7. Stress–strain relationship for the crystal (002) plane for the specimen with the elongation ratio of $\lambda = 300$.

to the applied stress. As to why the crystal lattice modulus cannot be determined precisely in this experiment even though the homogeneous stress hypothesis is valid here, it is probably due to the fact that lattice modulus is affected by the number of lattice defects, which cannot be eliminated in our sample preparation technique.

Figure 8 shows the results for specimen C-5, where curve a shows the intensity distribution in the stress-free state and curves b and c show the distributions of the sample under the stresses of 0.264 and 0.660 GPa, respectively.

Table I
Characterization of Specimens Used To Measure the Crystal Lattice Modulus

specimen	elongation ratio	crystal lattice modulus, GPa	crystallinity, %	crystal size, Å	orientation factor F_{200}	Young's modulus, GPa
A-1	50	222	90.4	350	0.99435	25–30
A-2	50	205	87.0	330	0.99569	
B-1	100	201	94.3	350	0.99980	45–55
B-2	100	225	90.0	400	0.99747	
C-1	200	213	92.3	330	0.99862	110–120
C-2	200	213	94.9	430	0.99899	
C-3	200	219	92.3	300	0.99985	
C-4	200	222	94.9	310	0.99957	
C-5	200	214	92.3	360	0.99792	
C-6	200	217	94.9	350	0.99756	
D-1	300	200	95.4	450	0.99999	151–202
D-2	300	215	95.4	380	0.99963	
D-3	300	229	96.2	430	0.99942	

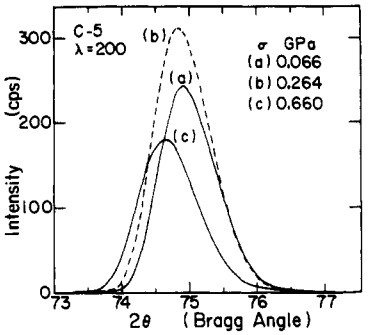

Figure 8. Intensity distribution of the crystal (002) plane under stress: (a) 0 GPa, (b) 0.264 GPa, and (c) 0.660 GPa.

The results show a gradual increase of intensity with increasing external stress up to the yield point, but it becomes lower as the applied stress increases beyond the yield point. Curve b corresponds to the preyielding state while curve c corresponds to the postyielding state. The behavior of curve b is probably due to a decrease of the amorphous fraction because of the stretch-induced amorphous–crystal transformation while the behavior of curve c is due to the increase of crystal lattice defects as a result of stretch-induced chain scission. Incidentally, it must be pointed out that the relationship between stress and crystal strain is reversible as long as the applied stress (or strain) is below the yield point.

Figure 9 shows the orientation distribution function $2\pi q_j(\cos\theta_j)$ of the crystal (002) plane for specimens A-1, B-2, C-1, and D-2. The data show a very sharp profile with a maximum value at $\theta_j = 0°$, indicating that the crystal c axes have a preferred orientation in the stretching direction. It is obvious from comparison of the results in the four functions that the degree of crystal x axis orientation increases with increasing elongation ratio λ, but even for the specimen with $\lambda = 50$, the degree of orientation is very high in comparison with those already reported for a number of drawn polyethylene materials. Therefore it is evident that a state of homogeneous stress can be achieved in our sample.

In order to further understand the homogeneous-stress hypothesis, we have also studied the possibility of whether the crystal lattice modulus may be affected by the crystallinity and crystal size in addition to the degree of crystal c axis orientation. Table I shows the results. These results indicate that the crystal lattice modulus is independent of crystal size and crystallinity. Incidentally, it should be noted that Young's modulus increases with increasing elongation ratio λ, but the maximum value for the specimen with $\lambda = 300$ is, at best, 202 GPa, which is lower than the value for the crystal lattice modulus.

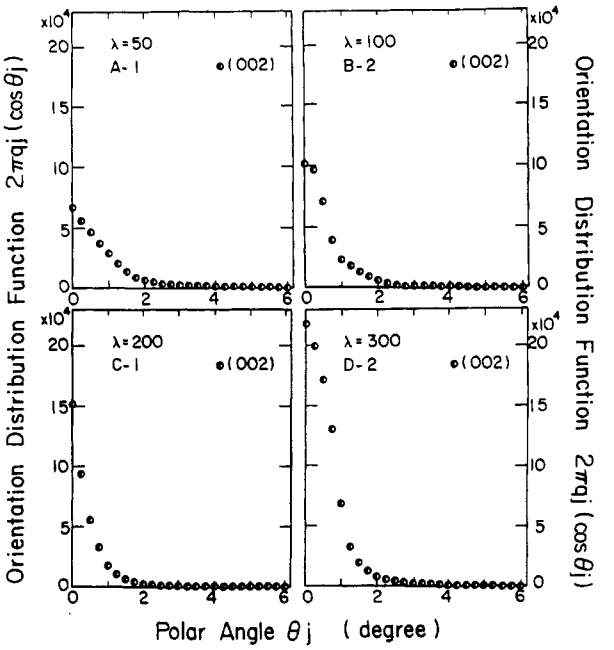

Figure 9. Orientation distribution function of $2\pi q_j(\cos\theta_j)$ of the reciprocal lattice vector of the crystal (002) plane of specimens with λ = 50, 100, 200, and 300.

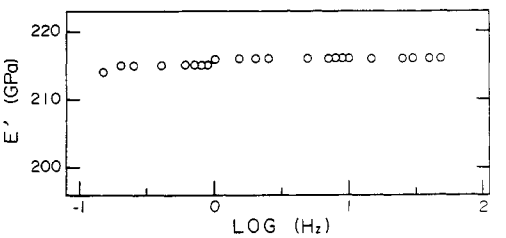

Figure 10. Frequency dependence of E' of a specimen with λ = 400 at 20 °C.

On the basis of the crystal lattice modulus measured in this experiment, an effort was made to produce specimens with a Young's modulus as high as the the crystal lattice modulus. Through trial and error, the following method is founded to be optimum. A specimen with $\lambda = 300$ was clamped in the viscoelastic spectrometer and subjected to sinusoidal strain over the frequency range 0.1–100 Hz at 140 °C. The process was repeated several times. In this manner, further elongation could be realized, resulting in a draw ratio of about 400. Subsequently, the specimens were cooled slowly to room temperature while still maintained in the stretched state. The complex dynamic tensile modulus was measured over the frequency range 0.1–100 Hz at 20 °C.

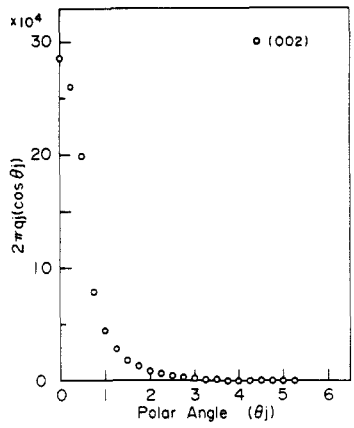

Figure 11. Orientation distribution function of $2\pi q_j(\cos\theta_j)$ of the reciprocal lattice vector of the crystal (002) plane of a specimen with $\lambda = 400$.

Figure 10 shows the real part E' of the dynamic complex tensile modulus as a function of frequency. The value of E' increases with increasing frequency and attains 216 GPa as the frequency exceeded 10 Hz. If one assumes that E' is approximately equal to Young's modulus, it may be concluded that this specimen has almost the ultimate elastic property of polyethylene. The orientation distribution function of the crystal c axes was almost unity as shown in Figure 11. However, we must emphasize that since the crystallinity of this specimen is 97–98%, Young's modulus cannot reach the theoretical value. It is estimated from our data that the crystal lattice modulus of this specimen is probably in the range between 220 and 229 GPa. The loss factor tan δ of this specimen at 20 °C was almost zero, so that the mechanical behavior is like that of metals rather than plastics. From the above experimental results, it is evident that one can easily produce bulk polyethylene films (or fibers) with Young's moduli close to the ultimate value. However, the tensile strength of these specimens was, at best, 6.2 GPa. It may be noted that unlike Young's modulus the tensile strength is in general more sensitive to the disorder of polymer chains within crystallites and to the existence of amorphous regions. In order to produce a specimen with a strength value higher than 10 GPa, the most important factor is probably to prepare a specimen with crystallinity exceeding 98% and with no lattice defects in the crystals. However, it would be a very difficult problem for polymer scientists.

Conclusion

From the above consideration, two main conclusions can be drawn.

First, the crystal lattice modulus was measured by X-ray diffraction using ultradrawn polyethylene films with elongation ratios in excess of 50. The modulus is in the range 213–229 GPa and is independent of the orientational degree, crystallinity, and crystal size as long as λ is greater than 50. These results indicate that a state of homogeneous stress can be achieved in the current experiment.

Second, on the basis of the measurable value of the crystal lattice modulus, efforts were made to produce a polyethylene film with Young's modulus close to the value of the crystal lattice modulus. Specimens with a Young's modulus of 216 GPa were obtained, which is close to the ultimate modulus value at 20 °C.

Acknowledgment. We thank Dr. Suehiro, Department of Polymer Chemistry, Faculty of Engineering, Kyoto University, for valuable comments and suggestions on producing an apparatus for measuring the crystal lattice strain shown in Figure 2. Thanks are also due to Prof. Ito, Kyoto University of Industrial Art and Textile Fibers, and Prof. Kaji, Kyoto University, Chemical Research Institute, who measured the crystal lattice modulus of polyethylene with Prof. Sakurada of Kyoto University about 20 years ago. They gave us valuable suggestions on carrying out the experiment.

Registry No. Polyethylene, 9002-88-4.

References and Notes

(1) Smook, J.; Torfs, J. C.; van Hulten, P. F.; Pennings, A. J. *Polym. Bull. (Berlin)* **1980**, *2*, 293.
(2) Capaccio, G.; Ward, I. M. *Polymer* **1974**, *15*, 233.
(3) Kojima, S.; Desper, C. R.; Porter, R. S. *J. Polym. Sci., Polym. Phys. Ed.* **1987**, *16*, 1721.
(4) Smith, P.; Lemstra, P. J.; Kalb, B.; Pennings, A. J. *Polym. Bull. (Berlin)* **1979**, *1*, 733.
(5) Barham, P. J.; Keller, A. *J. Mater. Sci.* **1980**, *15*, 2229.
(6) Smith, P.; Lemstra, P. J.; Booij, H. C. *J. Polym. Sci., Polym. Phys. Ed.* **1981**, *19*, 877.
(7) Smith, P.; Lemstra, P. J.; Pijppers, J. P. L.; Kiel, A. M. *Colloid Polym. Sci.* **1981**, *258*, 1070.
(8) Matsuo, M.; Manley, R. St. J. *Macromolecules* **1982**, *15*, 985.
(9) Matsuo, M.; Inoue, K.; Abumiya, N. *Seni-Gakkaishi* **1984**, *40*, 275.
(10) Sawatari, C.; Matsuo, M. *Colloid Polym. Sci.* **1985**, *263*, 783.
(11) Sakurada, I.; Nukushina, Y.; Ito, T. *J. Polym. Sci.* **1962**, *57*, 651.
(12) Sakurada, I.; Ito, T.; Nakamae, K. *J. Polym. Sci., Part C* **1966**, *15*, 75.
(13) Strobl, G. R.; Eckel, R. *J. Polym. Sci., Polym. Phys. Ed.* **1976**, *14*, 913.
(14) Holliday, L.; White, J. W. *Pure Appl. Chem.* **1971**, *26*, 545.
(15) Odajima, A.; Maeda, T. *J. Polym. Sci., Part C* **1966**, *15*, 55.
(16) Tashiro, K.; Kobayashi, M.; Tadokoro, H. *Macromolecules* **1978**, *11*, 914.
(17) Hermans, P. H.; Platzek, P. *Kolloid-Z.* **1938**, *88*, 68.